REPORT DOCUMENTATION PAGE

Form Approved
OMB No. 0704-0188

1. REPORT DATE *(DD-MM-YYYY)*	**2. REPORT TYPE**	**3. DATES COVERED** *(From - To)*
05-13-2008	Final Performance	09-01-04 to 07-31-07

4. TITLE AND SUBTITLE
High Yield Methods for Cutting Single-Walled Carbon Nanotubes

5a. CONTRACT NUMBER

5b. GRANT NUMBER
FA9550-04-1-0452

5c. PROGRAM ELEMENT NUMBER

6. AUTHOR(S)
Dr. Zhenning Gu, Dr. Kirk J. Ziegler, Dr. Howard K. Schmidt,
Ms. Zheyi Chen, Mr. Urs Rauwald, Dr. Robert H. Hauge, Prof. Richard E. Smalley and Prof. James M Tour
PI: Prof. James M. Tour
Co PI: Dr. Robert H. Hauge

5d. PROJECT NUMBER

5e. TASK NUMBER

5f. WORK UNIT NUMBER

7. PERFORMING ORGANIZATION NAME(S) AND ADDRESS(ES)

Carbon Nanotechnology Lab 6100 Main St., MS-100
Rice University Houston, Texas 77005

8. PERFORMING ORGANIZATION REPORT NUMBER

9. SPONSORING / MONITORING AGENCY NAME(S) AND ADDRESS(ES)
Air Force Office of Scientific Research - Chemistry and Life Science Directorate

10. SPONSOR/MONITOR'S ACRONYM(S)

11. SPONSOR/MONITOR'S REPORT NUMBER(S)

12. DISTRIBUTION / AVAILABILITY STATEMENT
UNLIMITED

13. SUPPLEMENTARY NOTES

14. ABSTRACT
Methods for cutting single-walled carbon nanotubes (SWNTs) to controlled lengths for material, biological and electronic applications are being developed. The research aims at establishing scalable cutting processes for preparing high quality short SWNTs with high yield, systematic procedure for evaluating the cutting results, and effective, scalable methods for length sorting of cut SWNTs. Caro's acid has been studied and chosen as the finishing cutting reagent. High temperature fluorination plus Caro's acid have been developed as our primary cutting method. Electron beam irradiation of ozonated SWNTs has shown promising cutting result. A standard procedure has been developed to individualize SWNT samples and to determine the length distribution. Preliminary results have indicated that phase separation technique could be a scalable, efficient means for length sorting of SWNTs. Ultra-short SWNTs (US-SWNTs) were produced by oxidation in oleum using fuming nitric acid.

15. SUBJECT TERMS

16. SECURITY CLASSIFICATION OF:			**17. LIMITATION OF ABSTRACT**	**18. NUMBER OF PAGES**	**19a. NAME OF RESPONSIBLE PERSON**
a. REPORT	**b. ABSTRACT**	**c. THIS PAGE**			Prof. James M. Tour
					19b. TELEPHONE NUMBER *(include area code)* 713-348-6246

Final Report to the Air Force Office of Scientific Research on "High Yield Methods for Cutting Single-Walled Carbon Nanotubes", grant number FA9550-04-1-0452

Prof. James M. Tour
Chao Professor of Chemistry, Professor of Mechanical Engineering and Materials Science,
Carbon Nanotechnology Laboratory
Smalley Institute for Nanoscale Science and Technology, MS 222
6100 Main St., Houston, Texas 77005
Phone 713-348-6246, fax 713-348-6250, e-mail tour@rice.edu

Summary of First Part of Research

This project has focused on cutting nanotubes into short tubes and sorting them by their length. The focus of most of the work has been based on using a high energy electron beam to introduce sidewall damage into the sidewall. While the final goal of this work has not been achieved, very recently obtained some promising results were obtained. The use of irradiation to induce sidewall damage has had slow progress. This has stemmed from the difficulties in functionalization and possible electron induced cross-linking which leads to difficulties in exploiting any induced sidewall damage. The process of fluorinating the sidewall of nanotubes is a well-understood process and seems to be easily controlled. However, irradiation of these samples showed no differences from the control sample. We, therefore, focused on the use of oxygenated functionalization. These chemistries are less mature and more difficult to characterize and control. Our efforts have focused on getting homogeneous functionalization using ozonation in various solvents. Irradiation of previous ozonated tubes, however, seems to have induced cross-linking of the tubes. We have, therefore, focused some effort at removing the cross-linking. However, this latest experiment used N_2 instead of air as a cooling gas and appears to have eliminated or at least significantly reduced the amount of cross-linking. Preliminary results of this latest experiment have shown that just 5 min of irradiation time (~10^{16} e^-/cm^2) yields short tubes with an average length of 83 nm compared to the starting length of 210 nm. This process only requires ozonation and irradiation (i.e. no Caro's acid step). An alternative approach that we have just begun to investigate is the use of SO3 to functionalize the sidewalls. This approach has the advantage that the functionalization can be easily reversed by reaction of the tubes with water.

During the course of the work on irradiated induced sidewall damage, there have been several significant discoveries while attempting to achieve this goal and are described briefly below:

- *Caro's Acid solutions for controlled cutting of damage sites*. Two years ago we were beginning to realize that the fluorination/pyrolysis approach would not be an ideal approach. We started to think of other means to introduce controlled amounts of damage sites into the sidewall. However, we did not have any means of exploiting sidewall damage in a controlled manner without introducing more sidewall damage. During the work on fluorinated and irradiated samples, we discovered that room temperature piranha solutions offer the ability to exploit sidewall damage in a controlled manner without introducing significant amounts of new sidewall damage. This has allowed us to have a

controlled cutting step that can take advantage of sidewall damage introduced through other processes. This process is a critical component of any cutting process currently being investigated.

- *Fluorination and Caro's acid cutting*. One of the first experiments we performed to introduce sidewall damage was utilizing fluorinated tubes. It was believed that the presence of the F atoms would allow carbon atoms to be removed from the sidewall by the formation of CF4 given the activation energy of the electron. Initial experiments focused on fluorination, irradiation, de-fluorination, and piranha treatment. During the work-up for this process, it was unexpectedly discovered that the control sample (no irradiation) yielded short cut nanotubes. Further work confirmed that fluorination followed by piranha (Caro's acid) was a viable approach to cutting. This is currently our primary means of cutting tubes.
- *Facile length measurements with software*. An inherent analytical step that is necessary for evaluating all cutting processes is the accurate measurement of nanotube lengths. We used to measure nanotube lengths by opening AFM images in SigmaScan software and simply tracing the cursor over each individual nanotube. However, this software package required significant user input (2 – 4 h) and was not able to systematically differentiate between individual nanotubes and nanotube ropes. Working with Smart Imaging Technologies, we developed a facile software program that is capable of measuring 1000+ nanotubes within minutes. Since the program utilizes the AFM image it is able to automatically differentiate the individual nanotubes from the nanotube ropes. This allows us to have a facile means of accurately measuring the lengths of a nanotube sample.

Another project of significance is the development of length-dependent extractions of nanotubes. Here we sought to develop a scaleable length-based separation technique. We developed a two-phase liquid-liquid extraction process which is capable of extracting water-soluble single-walled carbon nanotubes into an organic phase. The extraction utilizes electrostatic interactions between a common phase transfer agent and the sidewall functional groups on the nanotubes. Large length-dependent van der Waals forces for nanotubes allow the ability to control the length of nanotubes extracted into the organic phase as demonstrated by AFM. Further work should focus on the ability to perform step-wise extractions to get narrow distributions of lengths.

US-SWNTs

The production of ultra-short single wall carbon nanotubes (US-SWNTs) was achieved in research that was begun in this project and then overlapped with a subsequent project, "SWNT Composite Fibers (SCF)"grant number FA9550-05-1-0152. A summary of the US-SWNTs work comprises the second part of this report.

Detailed description of work

The general approach to cutting nanotubes described here is based on a two step process shown in Figure 1. The first step requires the introduction of carbon-carbon bond breakage in the lattice (sidewall damage) while the second process is aimed at exploiting these damage sites by locally etching the lattice to create short, cut nanotubes. A process capable of consuming the

damaged sites combined with a controlled means of introducing carbon-carbon bond breakage will allow the controlled cutting of SWNTs into short pristine segments. An important aspect to consider in the second step is the etch rate. Strong acid solutions heated to 40 – 70 ºC have been previously shown to create short nanotubes from long SWNTs.[1] These aggressive solutions are good at creating short length nanotubes; however, they typically result in significant losses due to fast etch rates. While this type of processing will indeed achieve short lengths, it does so by consuming the product from the ends. For example, if 100 nm length nanotubes were desired from a nanotube sample that has an average length of 1000 nm, then 90% of all the carbon has to be destroyed to obtain the desired product. Clearly this is not an efficient means to achieve short nanotubes. Cutting strategies should therefore attempt to achieve minimal carbon loss. Finally, these processes should not induce significant oxidation which may ultimately affect the electrical properties and usefulness of the SWNTs.[2]

Caro's Acid solutions for controlled cutting of damage sites

4:1 (vol/vol 96% H_2SO_4:30% H_2O_2) piranha solutions were prepared immediately prior to use to maintain their activity. The solution was then added to the nanotubes (1 mL piranha: 1 mg of nanotubes) once the solution was either cooled or heated to the desired temperature. Ammonium persulfate reactions were prepared by adding the nanotubes to 96% H_2SO_4 (1 mL solution: 1 mg of nanotubes). The tubes were stirred in concentrated acid for a minimum of 30 min to allow significant intercalation prior to introduction of the oxidant. Ammonium persulfate was then added to the mixture (1 g of the salt in 10 mL of 96% H_2SO_4). CAUTION: these oxidant solutions are very aggressive, corrosive solutions and appropriate safety precautions should be utilized including the use of acid resistant gloves and adequate shielding.

The nanotube/piranha mixture was stirred with a PTFE stir bar and immediately formed suspensions. The reactions proceeded for 15 min to 9 h (typically 1 h) and showed the evolution of gas. When the desired exposure was reached, the reaction was quenched by diluting the suspension with approximately 5 times the amount of NanoPure water resulting in a rapid rise in temperature. The solutions were quickly cooled to room temperature in an ice bath. This solution was then added to a separation funnel with a small amount of hexane. Ethanol (200 proof) was then slowly added, occasionally shaking, until the nanotubes were extracted into the hexane layer. The addition of too much ethanol, however, would result in the apparent expansion of the hexane layer making the separation of the aqueous phase more difficult. The two-phase mixture was allowed to settle for approx. 30 min and then the aqueous layer was drained from the funnel. After the initial separation, Nanopure water could be added to the funnel with the SWNTs remaining in the hexane layer. The nanotubes were then washed multiple times (4 – 5) until the pH was neutral. The remaining hexane solution was then filtered through 0.1 μm polycarbonate membranes (GE Osmonics), washed with ethanol, then hexane, and dried under vacuum at 50 ºC for 30 – 60 min.

The wet-air purification of nanotubes can be expected to introduce a small amount of sidewall damage. These nanotubes were utilized to study the effect of temperature on the etching at these damage sites. Piranha solutions consist of a mixture of sulphuric acid and hydrogen peroxide (4:1 vol/vol 96% H_2SO_4: 30% H_2O_2) and have been extensively utilized in the semiconductor industry to remove organic contaminants. The mixture of the two results in the formation of the strong oxidant H_2SO_5 (Caro's acid):

$$H_2SO_4 + H_2O_2 \leftrightharpoons H_2SO_5 + H_2O \qquad (1)$$

Figure 1a shows the average nanotube length determined from the histograms for nanotubes reacted with room (22 ºC) and high temperature (70 ºC) piranha solutions. The average nanotube length of the high temperature piranha solutions shows a decrease in length as the exposure time increases. After a 9 h treatment at 70 ºC, the average length is less than half of the original length. The average length for the room temperature treatment on the other hand shows an initial decrease and little changes in length from 1 h to 9 h of exposure to piranha. The weight loss associated with these reactions also shows a similar pattern as seen in Figure 1b. Nanotubes treated with high temperature piranha initially lose a significant amount of weight and then continually decrease reaching a weight loss of ~55% after 9 h. The weight loss of nanotubes treated with room temperature piranha, however, plateau at approx. 10 – 15% after only 1 h.

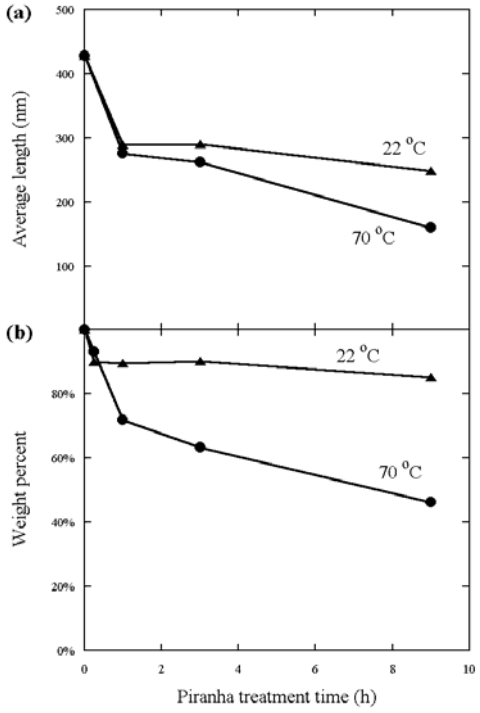

Figure 1. (a) Average nanotube length and (b) weight loss as a function of piranha treatment time for reactions at 22 ºC and 70 ºC. Reproduced with permission from *J. Am. Chem. Soc.* **2005**, 127, 1541-1547. Copyright 2005 Am. Chem. Soc.

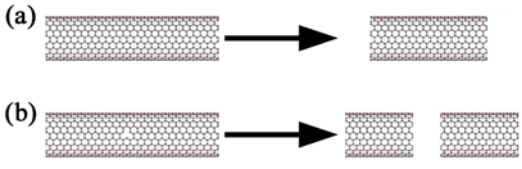

Figure 2. Schematic for etching of single-walled carbon nanotubes. This etching can occur from the (a) ends of the nanotubes or (b) at a damage site where carbon-carbon bond breakage has occurred.

The weight loss during piranha exposure clearly indicates that some of the nanotubes are consumed in the reaction. This etching can occur at the ends of the nanotubes or at sites where bond breakage has occurred in the graphene layer as seen in Figure 2. It is obvious from Figure

2 that significant length changes via etching at the nanotube ends would induce significant weight loss while etching at damage sites would result in shorter nanotubes with little weight loss. As seen in Figure 1, the room temperature piranha reactions indicate that the nanotubes have length changes of approximately 30% with only a 10% weight change. This data suggests that these strong oxidizing solutions are capable of etching at damage sites. The plateau in the length distribution of room temperature reactions suggests that the etching rate has been considerably slowed at room temperature having a rate on the order of 1 – 5 nm/h whereas high temperature piranha solutions have an etch rate on the order of 15 – 20 nm/h. The etch rates for graphite have been described as constant over the entire reaction[3-5] and SWNTs can be expected to behave similarly. Therefore, the initial change in the length distribution of over 100 nm in 1 h for room temperature piranha reactions confirms that etching has occurred at damage sites. Etching from the nanotube ends is still occurring at these reaction conditions but due to the slow etch rate this process will not induce significant changes in the length. In addition, high temperature piranha solutions were shown to increase the amount of sidewall damage while room temperature solutions had almost no increase in sidewall damage as determined by Raman spectra before and after the reaction.

At this point, it is clear that both room and high temperature piranha solutions are capable of etching at damage sites with high temperature piranha solutions creating more sidewall damage. The significant advantage of room temperature piranha solutions is the significantly lower carbon loss due to the decrease in the etch rate. Furthermore, high temperature piranha solutions are shown to preferentially etch away smaller diameter nanotubes.

At higher temperatures, an increased rate of consumption yields increasingly shorter nanotubes due to both cutting and etching of the nanotubes as witnessed by the Raman spectra for piranha treated nanotubes after H_2 treatment. The radial breathing modes (RBM), located between 150 – 300 cm^{-1}, are inversely dependent on the SWNT diameter[6] and are shown in Figure 3 for high and room temperature piranha solutions, respectively. The RBMs shown in Figure 3a show that the peak at ~267 cm^{-1} shows substantial decreases in relative intensity as the reaction time increases. This decrease in intensity suggests that smaller diameter nanotubes are being consumed or etched away under these reaction conditions. Indeed, it is expected that the smaller diameter nanotubes should be more reactive due to the higher strain induced on the lattice.[7-9] However, the RBMs of room temperature piranha solutions in Figure 3b show virtually no relative changes in the spectra after piranha treatment.

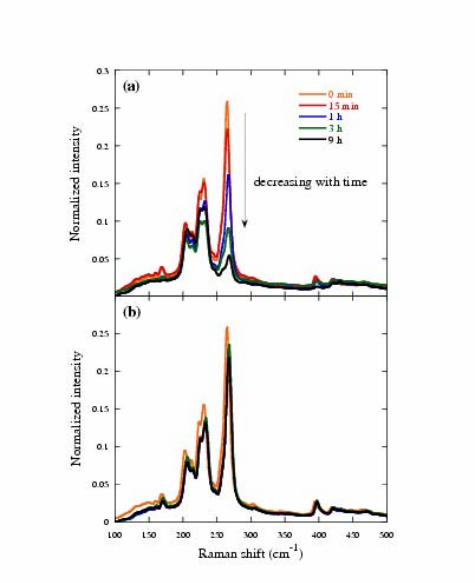

Figure 3. RBM Raman spectra (780 nm excitation) of dried SWNT powder after H_2 treatment as a function of piranha reaction time at (a) 70 ºC and (b) 22 ºC.

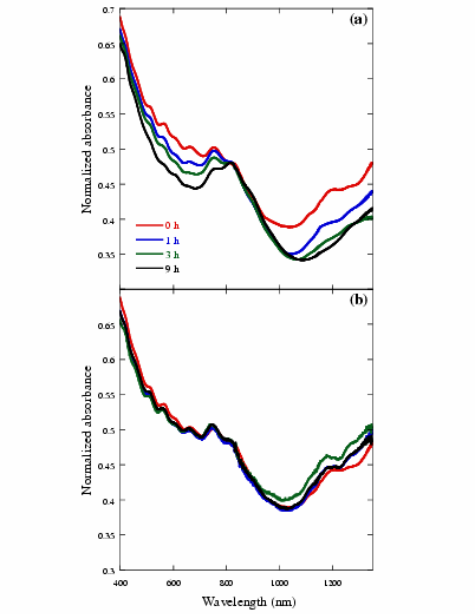

Figure 4. UV-vis-NIR specta after H_2 treatment for nanotubes treated in piranha at (a) 70 ºC and (b) 22 ºC at different reaction times.

UV-vis-NIR spectra on the room and high temperature piranha treatments after H_2 treatment, shown in Figure 4, also suggest that lower temperatures preserve the initial distribution of nanotube diameters in the sample. The 1-D nature of SWNTs results in diameter dependent van Hove maxima in the density of states resulting in sharp interband transitions associated with the singularities. The van Hove frequencies are diameter dependent with smaller diameter nanotubes having frequencies at lower wavelengths. The first van Hove frequencies of the high temperature piranha solutions (Fig. 4a) show substantial changes with reaction time in the absorption spectra at 1000 and 1200 nm which correspond to diameters of approx. 0.8 and

0.96 nm, respectively [7]. The second van Hove frequencies show similar changes in the intensities of the smaller diameter nanotubes confirming that selective oxidative etching of small diameter nanotubes is occurring at these reaction conditions. The UV-vis-NIR spectra of room temperature piranha solutions (Fig. 4b), however, confirm that no selective etching occurs at these reaction conditions.

Ammonium persulfate in 96% sulphuric acid has also been utilized for the cutting of SWNTs. This salt dissociates to form H_2SO_4 and H_2SO_5 (Caro's acid) similar to piranha solutions. The distribution of the cut SWNTs is nearly identical for piranha and ammonium persulfate solutions. The average measured length of the cut SWNTs varied by less than 10 nm. These ammonium persulfate solutions offer additional advantages over piranha solutions. These ammonium persulfate solutions maintain their oxidative strength better than piranha making the reactions easier to control. In addition, SWNTs can be stirred for long periods of time in H_2SO_4 where the acid is able to intercalate the nanotube ropes [10] before the addition of the oxidant. The dispersion of individual nanotubes ensures that all of the SWNTs will react with the oxidant. The addition of H_2O_2 (piranha solutions), however, would cause a significant temperature rise due to the heat of mixing (to 50 – 70 ºC) which results in significant carbon loss, increased sidewall damage, and selective etching of the small diameter nanotubes while the addition of ammonium persulfate can be maintained at ambient temperatures.

Conclusions

At high temperatures, piranha is capable of attacking existing damage sites and consuming the oxidized vacancies to create cut nanotubes. The SWNTs in these high temperature reaction conditions become increasingly shorter in length with an increase in reaction time. However, half of the starting material is lost to achieve these short length nanotubes. In addition, Raman and UV-vis-NIR spectra show that these reaction conditions result in the selective oxidative etching of the smaller diameter nanotubes. Room temperature piranha treatments also show the capability of attacking vacancies in the sidewall to achieve cut nanotubes. However, contrary to high temperature piranha solutions there is minimal carbon loss, no new sidewall damage, and no selective etching of the nanotubes. Therefore, room temperature piranha solutions offer the ability to exploit active damage sites in the sidewalls of the nanotube in a controlled manner without counterproductive destruction of the nanotubes. In conjunction with methods used to induce controlled amounts of damage sites, these room temperature piranha solutions have the potential to yield an efficient means of creating short, cut nanotubes useful for many electronic, biological, and materials applications.

Fluorination and Caro's acid cutting

The fluorination of nanotubes was done in a similar manner to previously published approaches [11, 12]. The nanotubes were exposed to a 10% F_2 in He gas mixture at approx. 150 ºC for 8 – 12 h. The carbon to fluorine ratio was determined by XPS to be ~C_2F. De-fluorination was achieved by suspending the fluorinated nanotubes in isopropanol and reacting them with 35% hydrazine in water for 1 – 2 h. Typically, after de-fluorination the nanotubes were reduced to ~$C_{10}F$. The de-fluorinated SWNTs were then reacted with room temperature piranha solutions as described above. The fluorine content in the final cut nanotubes was below the detection limit.

Recently, STM analysis of the pyrolysis of fluorinated nanotubes showed that as the fluorine was slowly removed from the nanotube during pyrolysis some defect sites remained behind [13]. As the temperature was increased, pyrolysis occurred at these defect sites resulting in cut nanotubes. This data suggests that the fluorination of the nanotubes at elevated temperatures results in some carbon-carbon bond breakage during fluorination. It is believed that thermal fluctuations during fluorination will create hot spots that have sufficient activation energy to form CF_4 and leave a vacancy in the nanotube sidewall. Indeed, fluorination at very high temperatures has been shown to completely destroy the nanotubes [12]. In order to eliminate the coalescence problem associated with high temperature pyrolysis, these nanotubes were reacted with Caro's acid to exploit the vacancies. The complete cutting strategy is depicted in Figure 5. The fluorination is carried out until ~C_2F is achieved. Prior to the reaction with Caro's acid the fluorine had to be removed from the nanotubes to make the nanotubes wettable with piranha. De-fluorination of the SWNTs is achieved by reacting the fluorinated nanotubes with hydrazine which has been previously shown to remove a majority of the fluorine [12]. After fluorine removal, the vacancies created during fluorination have been exposed and can now be exploited using room temperature Caro's acid solutions.

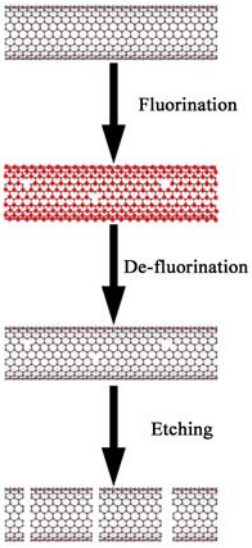

Figure 5. Cutting scheme using fluorination to induce carbon-carbon bond breakage.

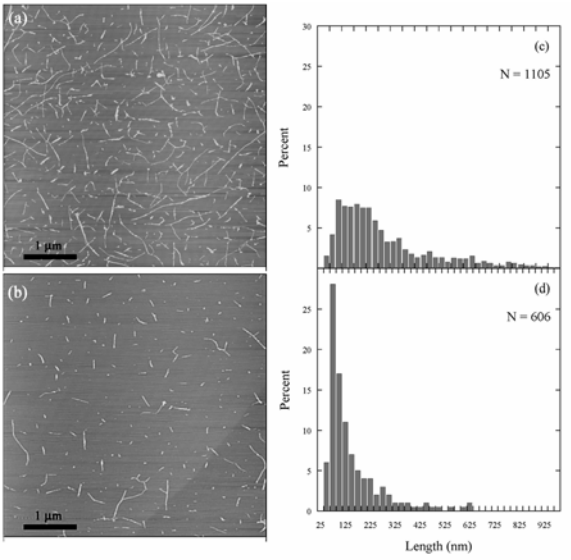

Figure 6. AFM image and corresponding histogram for de-fluorinated C_2F nanotubes (a,c) before and (b,d) after Caro's acid treatment.

Figure 6 display the AFM images and corresponding histograms for the nanotubes before and after Caro's acid treatment. Prior to the Caro's acid reaction, the de-fluorinated nanotubes show no apparent damage sites and have an average length of 300 nm. After ~1 h of room temperature Caro's acid treatment, however, the average nanotube length has decreased to ~100 nm. Un-fluorinated control samples give an average length of ~ 275 nm (not shown) indicating that damage sites are introduced through the fluorination process. Recall that these room temperature Caro's acid solutions have a very slow etch rate on the order of 1 – 5 nm/h. This slow etch rate suggests that a significant amount of vacancies were created during the fluorination process and subsequently exploited with Caro's acid. The fluorination-based cutting process has been shown to be a very efficient process with an overall carbon yield of 70 – 80%.

Conclusions

The fluorination-based cutting strategy has been shown to be an effective, controlled process with a high yield of short, cut nanotubes. The process involves fluorination to ~C_2F which creates carbon-carbon bond breakage in the form of sidewall vacancies. These vacancies can then be exploited through the use of room temperature Caro's acid solutions to achieve short, cut nanotubes. The overall carbon yield for the fluorination cutting strategy is typically 70 – 80% and the final average length of the nanotubes is approx. 100 nm. However, this approach is unable to control the lengths of the nanotubes by more than 10 – 20 nm. Therefore, we have continued our search for a controllable means on introducing sidewall damage.

Facile length measurements with software

While some progress has been made with in-situ techniques[14-16], these approaches typically only give an average length and no information about the distribution. Direct imaging techniques are more tedious but typically give more information. Of these imaging approaches, AFM appears to be the most useful technique [1, 17]. However, accurate measurements require two key steps: (i) suspension of the individual nanotubes in a solvent for dispersion onto a substrate and (ii) the length measurement of a statistically significant number of nanotubes. Many prior

reports have utilized AFM as a means of measuring the length distribution but rarely have more than 100 nanotubes in their population. This stems from the difficulties in achieving the suspension of individual nanotubes and the tedious nature of measuring the length of 1000+ nanotubes. Here we describe a simple and efficient means of measuring a large population of nanotube lengths.

The first key step to length measurement analysis is the suspension of the nanotubes. Many functionalization chemistries involve significant processing and/or give few individual nanotubes and a large portion of small bundles. The use of surfactants followed by centrifugation [18, 19] yield a significant amount of individuals but does not give an accurate representation of the sample since the solution is decanted from the solids. Extensive and intense sonication may also seriously distort lengths due to sonication induced cutting of nanotubes.

The recent development of Billups Li/NH3 chemistry on nanotube sidewalls have significantly aided the dispersion of nanotubes. For length analysis, dilute solutions are used to obtain the correct surface coverage for image analysis. These suspensions can then be spin-coated onto freshly cleaved mica substrates after brief, mild sonication (~1 min) yielding a high quantity of individual nanotubes as seen in AFM images.

The second critical step is the measurement of a large population of nanotubes to achieve statistically meaningful lengths. The lack of a method that yielded high quantities of individuals often precluded the analysis of a significant number of nanotubes. These low yields would have required numerous AFM images to be collected to obtain statistically significant length measurements. The high yield of the Billups reaction allows the measurement of 1000+ nanotubes by the collection of a handful of images. To eliminate the tedious nature of manually measuring 1000+ nanotubes, the lengths are measured using the Nanotube Length Analysis module of the SIMAGIS (Smart Imaging Technologies, Houston, Texas) software package. This new software package automatically analyzes multiple AFM images to obtain statistically accurate length and height (diameter) measurements of the nanotubes contained in the sample as well as particle and SWNT rope populations. In less than 1 minute, the software can analyze a single AFM image and extract the relevant length and height information for analysis.

As can be seen in Figure 7b, the program is capable of recognizing the nanotubes in the image and tracing their lengths. The program is also able to simultaneously obtain an average height along the length of the nanotube; therefore, the final image differentiates individual nanotubes (green) from nanotube ropes (black). Typically, nanotubes with heights smaller than 2 nm are considered to be individuals due to the presence of the dodecyl chains. The 2 nm height limit is stringent and likely excludes some individuals from larger diameter nanotubes but is necessary to eliminate ropes of small diameter nanotubes. Combining the statistics for individual nanotubes and ropes (bundles) as seen in Figure 8 indicates that these bundles typically consist of less than five nanotubes. The shaded region indicates those nanotubes considered to be individuals. The data shows that 92% of the nanotubes measured are individuals. Similar measurements on other samples indicate that dodecylation via the Billups reaction typically achieves 75 – 90% individuals. In addition, there is no length effect on nanotube de-bundling suggesting that the Li used in the Billups reaction is indeed capable of intercalating the graphene layers even for very long nanotubes allowing sufficient sidewall attack of the alkyl radicals. Finally, the program will also identify particles within the images as seen in Figure 9 (shown in red on Figure 7). For example, the data distinctly indicate the presence of a bimodal distribution. This allows the analysis of metal catalyst particles and fullerenes present in raw nanotube samples which may give insight into growth processes.

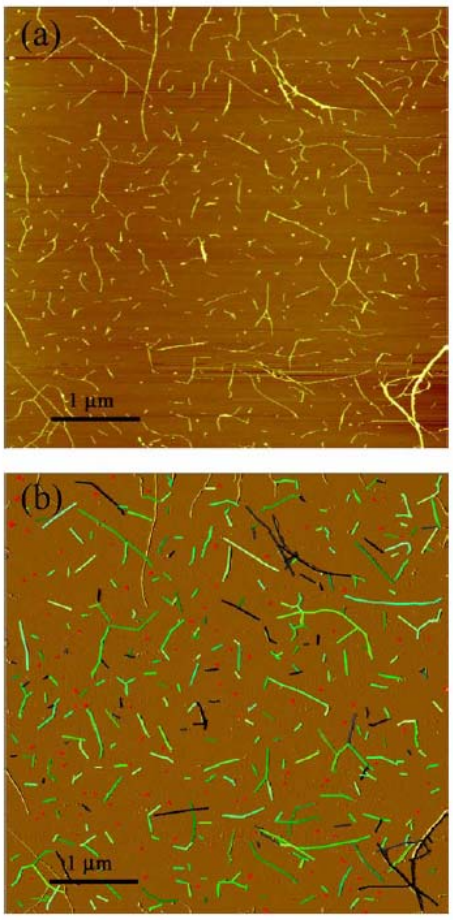

Figure 7. (a) AFM image of nanotubes functionalized with dodecyl chains using the Billups chemistry. Note the high concentration of individual nanotubes that are dispersed on the mica substrate. (b) Nanotubes measured using the Nanotube Length Analysis package of the SIMAGIS software. Individual nanotubes are designated by a green color while the nanotube ropes are shown in black. Particles are also shown in red.

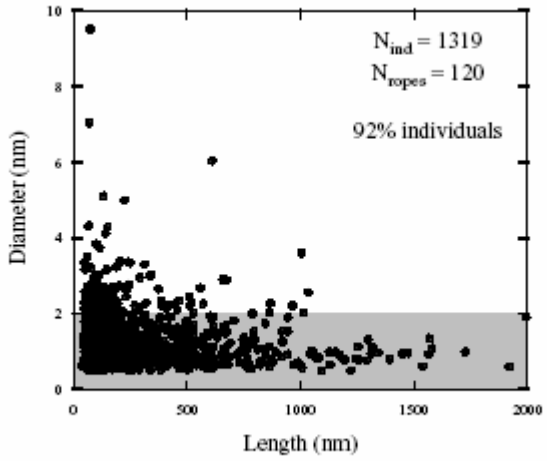

Figure 8. Length and diameter distribution of dodecylated single-walled carbon nanotubes. The gray box indicates those nanotubes considered to be individuals. The distribution indicates that 92% of the sample exists as individuals.

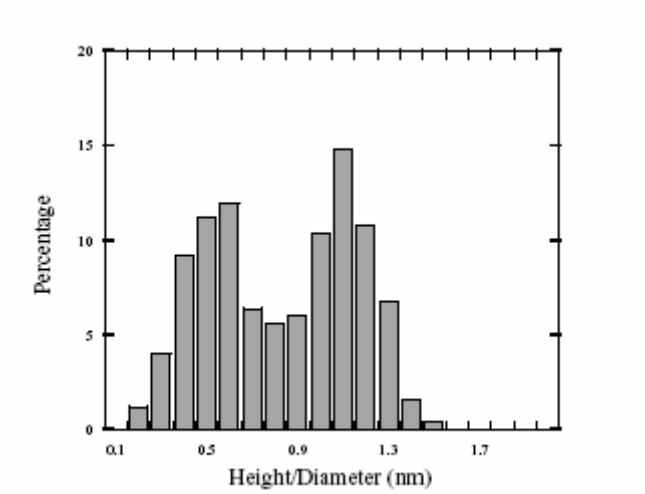

Figure 9. Particle distributions from multiple images of the sample shown in Figure 7.

In order to achieve accurate measurements and minimize user input, quality AFM images are crucial. Poor image quality can have drastic effects on the quality of the nanotube traces. For example, images that have a 'grainy' background will often yield ghost nanotubes. Other common AFM image artefacts will also yield false nanotube traces. The resolution of the image will affect the smallest length of nanotubes that can be accurately measured. Therefore, all AFM images should be taken at the maximum resolution at a scan size capable of visualizing both the longest and shortest nanotubes in the sample. In addition, it is important to achieve the appropriate surface coverage. Although the software package can distinguish overlapping nanotubes, too high of surface coverage can cause significant problems. After the program traces the nanotubes in the AFM image, the user has the option of manually editing the trace lines. However, if the surface coverage is chosen correctly, manual adjustments are insignificant. Although numerous adjustments were made to the image with moderate surface coverage, the errors encountered changed the final measured length by less than 10%. This is not true for higher surface coverage images which can change by 30% or more. Interestingly, the distribution does not change significantly after the manual adjustments. However, the tail of the distribution has considerably more long nanotubes suggesting that it is more difficult to measure the longest nanotubes. These nanotubes will have considerable overlap leading to erroneous nanotube traces. Therefore, shorter nanotube samples typically give more accurate results with minimal need for manual adjustments. To keep the user input to a minimum, a moderate surface coverage is the optimal choice. It maximizes the ability of the software to differentiate between overlapping nanotubes while being able to get significant statistics with a bare minimum of AFM images and user intervention.

Conclusions

The functionalization of SWNTs with dodecyl chains via a Billups reaction yields as high as 92% of the sample as individual nanotubes in a chloroform suspension. These suspensions can be utilized for AFM image analysis. With moderate surface coverage and quality AFM images, the Nanotube Length Analysis module of SIMAGIS is capable of differentiating between individual nanotubes, nanotube ropes, and particles with minimum user intervention. Analysis of multiple AFM images (<10), therefore, allows the measurement of a significant population of the sample obtaining an accurate length and diameter measurement of the sample.

Irradiation induced sidewall vacancy formation

Irradiation is being investigated to introduce vacancies because the distance between vacancies (and, hence, the length of cut tubes) should be controlled by the irradiation density (dosage). Initial investigations into irradiation induced sidewall damage looked at both gamma and electron irradiation. We have determined that gamma irradiation was too costly for the dosages that would be required to create enough vacancies in the nanotubes. It was determined that the primary mode of gamma radiation interaction would be Compton scattering where the photon hits an electron with a portion of its energy being transferred. Gamma irradiation can be done at two STERIS sites using Co-60 sources (1.17 MeV). The site in El Paso, Texas is for bulk-scale samples in Al canisters (approx. 2' X 3' X 10') and Robert Bettis is in charge of the facility (915.855.2001, ext 316). The other site in Morton Grove, IL is for testing and prices are based per box (up to 1 kg). The contact at Morton Grove is Betty Howard (847.966.1160; Betty_Howard@steris.com). Pricing for samples less than 20 kGy is ~$470/box; 30-35 kGy is ~$880/box; and 50 kGy is ~$1450/box. Minimum order is $785. Typical doses for medical sterilization are 25 kGy. Routine analysis is listed as 7 – 10 days. However, typically turnaround times are faster. Priority analysis can be done in 1 – 3 days. Samples are run in a batch process.

Compared to gamma irradiation, electron beam irradiation has reduced penetration depth requiring larger beam energies. However, electron beam irradiation is more cost effective but also has further limitations with heat rise. Electron beam irradiation should be cheaper and more easily integrated into future bulk-scale production of nanotubes. Electron beam irradiation can also be done at the STERIS Libertyville, IL facility (5 MeV). The electron beam is on continuously and is accelerated using microwaves; it is 8 cm in diameter and scans across a 126 cm path at a rate of 100 Hz. The samples are loaded onto a conveyor that can be run at speeds from 0 – 50 ft/min. The electron beam achieves a power of 80 kW with a current of 16 mA yielding a current density of approximately 2×10^{15} electrons/s·cm^2. Dosage adsorbed is determined using radiochromic film, which is a 1 cm^2 plastic-coated radiation-sensitive dye strip that can be read spectroscopically to yield doses in kGy. Irradiation occurs under ambient atmospheric conditions. Our samples can be placed in a flat tray (1" thick) or in ½" diameter vials (based on density of 0.2 g cm^{-3} and run through their conveyor system. Samples in the flat tray will experience a 'spike' approximately ½ through the sample due to Compton scattering. Higher doses will be passed through multiple times to increase dosage uniformity and reduce heat rise. Frank Rich (847.247.0970; Frank_Rich@steris.com) is the sales representative at STERIS and Chad Rhodes (847.265.1920) is the technical expert. For samples up to ~ 1 kg, 50 kGy is $800; 100 kGy is $1250; and 250 kGy is $1500 – 1750. Higher dosages are achievable but need quotes based on material properties.

For small scale experiments, we have been working with Donald Klosterman (937.229.2528; Donald.Klosterman@udri.udayton.edu) at the University of Dayton Research Institute on the electron induced introduction of sidewall damage. This facility has a pulsed 300 W, 3 MeV electron beam. This facility operates similar to the STERIS electron beam with a conveyor system (20 – 50 cm/min typical) where the dosage is measured using radiochromic film.

The e-beam source is a 3 MeV pulsed linear accelerator with linear scan horn. This system generates a high energy beam of electrons that is directed vertically downward and is

swept into a linear curtain. The apparatus is contained in a concrete vault in order to shield the operators from the e-beam radiation as well as X-rays that are indirectly created in the process.

The e-beam accelerator is a device that generates free electrons and accelerates them to near relativistic speeds in a high vacuum chamber. The electron beam will experience too much attenuation during acceleration if the pressure is greater than 10^{-6} torr (1.33×10^{-4} Pa), with a pressure of 10^{-7} to 10^{-8} torr (1.33×10^{-5}-1.33×10^{-6} Pa) being more typical. In the pulsed linear accelerator (pulsed linac), a tungsten-barium composite "dispenser" cathode is heated to 1100°C and pulsed with a 25 kV current. The pulse rate can be adjusted from 25 to 250 pulses per second (pps). Each pulse generates a concentrated, 5-microsecond-long packet of electrons near the head of an accelerating cavity. The accelerating cavity receives high-power 3 GHz microwaves that are generated by a magnetron and propagated through a waveguide. The magnetron is also pulsed with a separate 25 kV current, such that the microwaves resonate in the accelerating cavity as a standing wave that is synchronized with the pulsing of the cathode. Voltage gradients created by the electromagnetic (E-M) standing wave exert a downward force on the electron "packets" such that they are accelerated to several MeV.

The electron beam emerges from the accelerating cavity in the form of discrete packets traveling linearly downward and is approximately the diameter of a pencil. As it enters the scan horn, the beam is swept back and forth in the X-direction by an electromagnet ("scanning magnet") operating at 25 Hz. The beam is thus converted to a linear curtain as it travels through the scan horn. The e-beam curtain emerges from the scan horn through a 1.5-micrometer-thick titanium foil "window" and enters the atmosphere. The beam impinges the nanotubes which are located on a glass frit located approx. 10 inches below the scan horn (12 inches to table). The electrons pass through the target and eventually are collected by a metal cart. The beam current (i.e. related to the # electrons per unit time) can be directly monitored by an oscilloscope that measures the voltage drop across a 100-ohm resistor placed between the cart and ground. An effective beam diameter of 5 cm was arbitrarily assigned by visual inspection of the dosage curves.

We have prepared sample holders for the pearls during irradiation shown in Figure 10. These holders are constructed of aluminum and have an I.D. of approx. 2 inches. The holders are designed to allow a bed height of 1 inch or approximately 10 g of nanotube pearls. Inlet and outlet connections are available to allow for air-cooling during irradiation. The inlet has an air distributor designed to minimize turbulence. The heat rise is minimal with a gas flow rate of 25 SLM. A temperature below 100 °C can be maintained. For long irradiation times, the beam is occasionally turned off to allow the sample to cool.

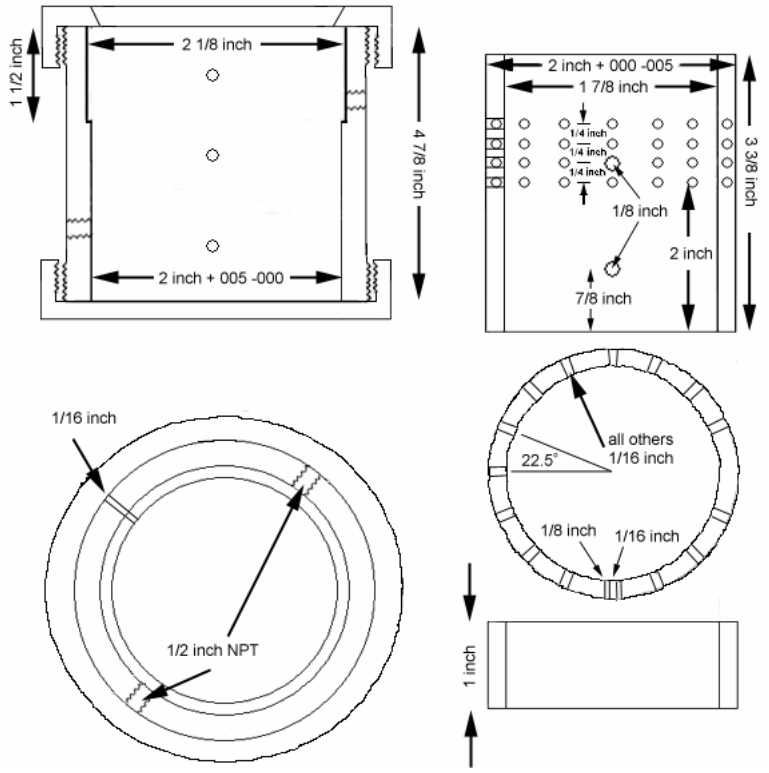

Figure 10. Schematic for aluminum holders utilized for irradiation experiments.

Radiation is measured as a dosage defined as the energy (J) of radiation absorbed per unit mass (kg) of material. The SI unit of dose is "Gray" (Gy), where 1 Gy is equal to 1 J/kg, and 1 kGy is equal to 1 kJ/kg. Dose is related to the cumulative number of electrons that have passed through a material, as well as the energy of the electrons. The dose will vary throughout a solid body because the scan horn may not evenly sweep the electron beam (X direction non-uniformity), the sample may not be translated symmetrically under the scan horn (Y direction non-uniformity), and because the electrons lose energy as they travel through the material (Z direction non-uniformity). Thus, dose distribution must be determined as a function of all three spatial coordinates, X, Y, and Z. It is standard practice to specify the "dose" applied to a material as the dose measured at the surface of the material. It is normally feasible to adjust the machine parameters to deliver a dose uniformity of ±10% over the entire X-Y area of a sample.

Electron beam irradiation can result in the expulsion of C atoms from the nanotube lattice if the energy of the electrons is greater than 86 keV. However, the cross-section of these events is very small. The more likely event to occur during irradiation is the ionization of the atoms (cross section of 10^6 vs. 10^2 barn). For metals or semiconductors, however, the charge is spread across all atoms faster than bond re-ordering can occur. Therefore, the irradiation of pristine tubes is limited to low probability direct knock-on events due to the fast dissipation of ionization events. Irradiation of pristine tubes requires very high dosage rates to induce significant damage. The use of functionalized nanotubes in irradiation experiments should allow ionization and sufficient activation energy to induce vacancies in the sidewall of fluorinated, epoxidized, or sulfonated tubes.

Fluorinated tubes showed no irradiation induced vacancies that could be exploited by room temperature piranha solutions. Interestingly, the control experiment (no irradiation) for this investigation lead to the discovery that fluorinated tubes followed by piranha (Caro's acid)

could yield short, cut nanotubes. Recent efforts have focused on oxygen-containing functional groups such as epoxides or sulfonate groups. The ozonation of nanotubes has been performed in methanol solutions at dry ice/acetone temperatures. However, these reactions are dangerous due to the creation of unstable ozonides which can be explosive when warmed. Therefore, ozonation of nanotubes in perfluoropolyether (PFPE) solvents was explored due to their high solubility of oxygen/ozone. The high solubility offers the advantage of achieving significant ozone concentrations at room temperature. Extensive ozonation of the nanotubes can be achieved in these PFPE solvents. This route appears to be the most efficient means of introducing a homogeneous dispersion of epoxide groups into the sidewall of all nanotubes.

The irradiation of these ozonated tubes are expected to cause localized heating events that will result in a reaction evolving CO and/or CO_2. This reaction will result in the formation of a hole in the nanotube sidewall. Irradiation of ozonated tubes via PFPE (3 MeV beam receiving approximately 10^{16} e^-/cm^2) appears to induce cross-linking of the tubes as witnessed by AFM. However, recent experiments suggest that the use of N2 as a cooling gas may help to minimize or eliminate the formation of cross-linking (discussed further below).

Using air as a cooling gas, Raman spectra for all ozonated and irradiated samples show that the Billups alkylation reaction is not able to functionalize the sidewalls sufficiently as seen in Figure 11. The D band shows no increase after functionalization and the functionalized tubes cannot be suspended in CHCl3. Note that the non-irradiated control sample is able to be functionalized and suspended.

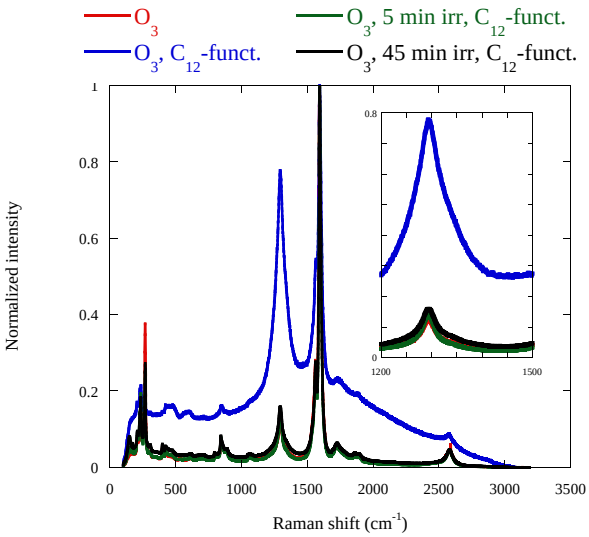

Figure 11. The effect of irradiation on the Billups functionalization reaction. Note that all irradiated samples cannot be functionalized as characterized by the low D/G to ratio.

Caro's acid solutions cannot be utilized on any ozonated samples. It appears that the environment is too aggressive and likely destroys most of the tubes. Therefore, epoxides were removed with triphenylphosphine and the tubes are already shorter as seen in the histogram in Figure 12. The histogram shows that nearly 85% of the tubes are shorter than 100 nm in length. However, these samples had a significant amount of aggregation that could be witnessed in the solutions likely due to the cross-linking. Therefore, approaches at reversing the cross-linking have been investigated. It appears that the use of H2 at 500 ºC is capable of reversing the cross-

linking allowing the Billups reaction to occur on these samples. It is possible that the selection of gas utilized may not be important. Therefore, further work should investigate the use of Ar or other gases.

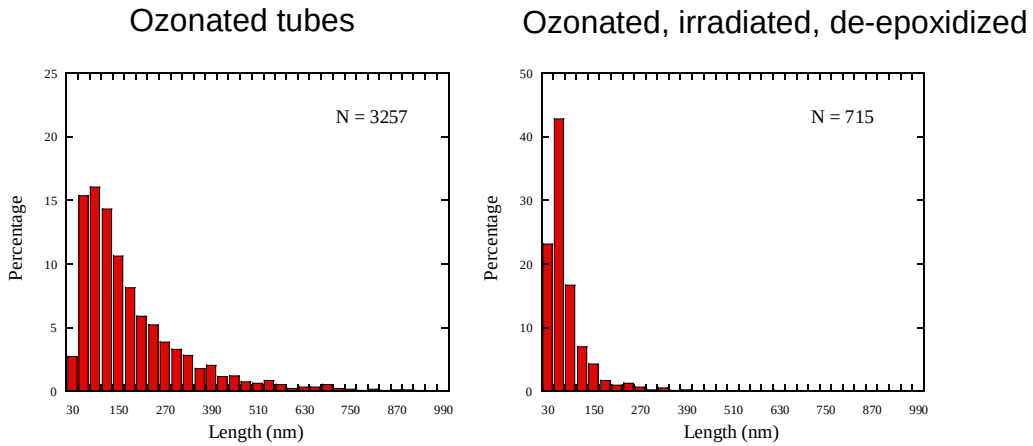

Figure 12. Length measurements for nanotubes ozonated in PFPE and after irradiation and de-epoxidation. Note that nearly 85% of the final cut tubes are below 100 nm.

Our most recent experiments utilized N2 as a cooling gas. These experiments had no difficulties in functionalizing the tubes via the Billups reaction. This suggests that the extent of cross-linking has been significantly minimized or possibly eliminated. The AFM and length measurements of these samples shows similar lengths to the previous results after only 5 min (10^{16} e^-/cm^2) or irradiation time. However, the apparent minimization of the cross-linking is a significant improvement. Work is underway to measure the nanotube lengths at longer irradiation times to see if we can control the length by controlling the irradiation time.

Conclusions

It is apparent that ozonation and electron irradiation can yield short, cut tubes. However, the electron-induced cross-linking of the tubes and the aggressive nature of Caro's acid on these tubes has made progress slow. Our most recent results, however, suggest that we have at least minimized the cross-linking. In a rather simple 2-step process, cut tubes can be obtained. The fact that a low dosage of electrons may be utilized to cut the tubes and that Caro's acid is not required makes this process more economical than previously envisioned.

Length-dependent extraction of nanotubes

Concentrated nanotube solutions in water were prepared without the use of surfactants by functionalizing the sidewalls of the purified nanotube with chloroaniline sulfonate. To obtain a higher degree of functionality, the nanotubes were functionalized multiple times to obtain a functionality ratio of approx. 1:18 as determined by TGA. These functionalized nanotubes have high solubility in water and reasonable solubility in other polar solvents (e.g. methanol, ethanol). The nanotubes were dissolved in water (0.04 – 0.2 mg/mL) and placed in a vial. Then, a solution of TOAB in an organic solvent (either ethyl acetate or toluene) is added to the vial at a 1:1 volume ratio resulting in a liquid-liquid phase system. The vial is shaken vigorously by hand for

30 s to increase interfacial area and assist transfer across the interface. After the two-phase mixture is vigorously shaken, the system is filled with grey emulsions. With an excess of TOAB, the emulsions settle and complete extraction of the nanotubes into the organic layer has occurred. The emulsions formed in toluene systems coalesced within a few minutes while those formed in ethyl acetate systems took considerably longer.

The collected SWNTs in the organic layer could not be re-suspended in water but could be easily transferred back to an aqueous or alcohol solution by reversing the reaction. The TOAB ligands are de-complexed by the addition of an excess of 96% acetic acid to the organic phase, which apparently causes the TOA^+ to preferentially bind to the acetate anions. The solution was then stirred for 20 – 30 s resulting in the immediate formation of aggregated particles, filtered through a 0.2 μm PTFE filter membrane, and washed 3 – 5 times with ethanol. The nanotube powder was then collected and re-suspended in water, methanol, or ethanol after ultrasonication for ~1 min.

Length-dependent extractions are obtained by utilizing a substochiometric ratio of TOAB. Emulsion formation became more problematic at these conditions. The emulsions settle slowly (over ~2 hours) still giving a water phase swollen with emulsions that were stable for days. When ethyl acetate is used as the organic solvent, very fine emulsions fill the swollen water phase occupying almost the entire liquid volume while toluene systems form emulsions that are coarser. The high conductivity of the swollen emulsion phase suggests that it is a water continuous phase. The high surface activity of the partially complexed SWNTs is likely due to the significant number of charged sites that remain as well as the significant number of hydrophobic sites rendering the SWNT an amphiphobic surfactant.

Due to the significant number of charges remaining on partially complexed SWNTs, the SWNTs could not be extracted into the organic phase. Therefore, salts such as ammonium chloride were used to charge neutralize the remaining sulfonate anions. The ammonium cations will allow charge neutrality to be achieved without increasing the organophilicity of the nanotubes. While emulsion stability was significantly diminished, dilute TOAB solutions still remained problematic. Several approaches were attempted to break-up the formation of emulsions including pH changes, temperature changes, the addition of salts and co-solvents, and centrifugation. Of these approaches, only freezing was found to effectively break the emulsions. After thawing the two-phase system, the carbon nanotubes are transferred to the organic phase after gentle agitation.

Figure 13 shows the extraction of nanotubes with varying concentrations of TOAB. No extraction of the SWNTs occurs without TOAB (vial **1**). At low TOAB concentrations (vial **2**), there is insufficient complexation to render the nanotubes organophilic and very few nanotubes are extracted. However, the complexation of the TOAB to the nanotubes has rendered the SWNTs hydrophobic. Therefore, these solutions tend to form a very stable emulsion/interphase that cannot be broken up even after freezing. An increase in the concentration of TOAB shown in vials **3** and **4** results in the extraction of a small amount of nanotubes into the organic layer. Continued increases in the TOAB concentration (vials **5** thru **7**) causes enough complexation that a significant portion of the nanotubes have become organophilic enough to be extracted into the organic layer. Finally, complete complexation of the nanotubes results in the extraction of all nanotubes (vials **8** and **9**). UV-vis-NIR absorbance spectra (Shimadzu UV-3101PC spectrometer) of the upper organic phases confirm that the concentration of TOAB that extracts all of the nanotubes corresponds to the theoretical for a 1:1 stoichiometric electrostatic

interaction. No extraction of nanotubes occurred without the presence of the functional groups on the SWNTs or without the TOAB.

Figure 13. The effect of TOAB concentration on the extraction of SWNTs into an ethyl acetate phase. (a) The solutions before and (b) after extraction. The TOAB:SO_3^- ratio for vials **1** – **9** are 0, 0.15, 0.3, 0.45, 0.6, 0.75, 0.9, 1.0, and 2.0, respectively.

For length measurements of the extracted organic layer, the organic phase was collected, washed with acetic acid as described above, and re-suspended in methanol after ultrasonication for ~1 min. The extracted nanotube solutions were then spin-coated onto freshly cleaved mica substrates yielding a high quantity of individual nanotubes. Figure 14 shows the length distributions for the starting material and for extractions at stoichiometric ratios (TOAB: SO_3^-) of 0.3, 0.4, 0.6 and 0.75. Only individual nanotubes were utilized for length measurements. Typically, over 1000 nanotubes were measured to obtain statistically meaningful results. The starting material (Fig. 14a) has a broad distribution of nanotube lengths with an average of 282 nm. The addition of enough TOAB to complex 30% of all SO_3^- moieties with TOA^+ results in only very short nanotubes being extracted into the organic layer as seen by the AFM and corresponding histograms (Fig. 14b). As can be seen, the length distribution narrows considerably with 81 % below 100 nm and an average length of 73 nm. Increased ion-pairing results in longer nanotubes being extracted. After 75% of the SO_3^- moieties are ion-paired, the length distribution begins to approach that of the starting material. It is evident that the average length increases monotonically with TOAB concentration and approaches the average length of the starting material (square symbol in figure).

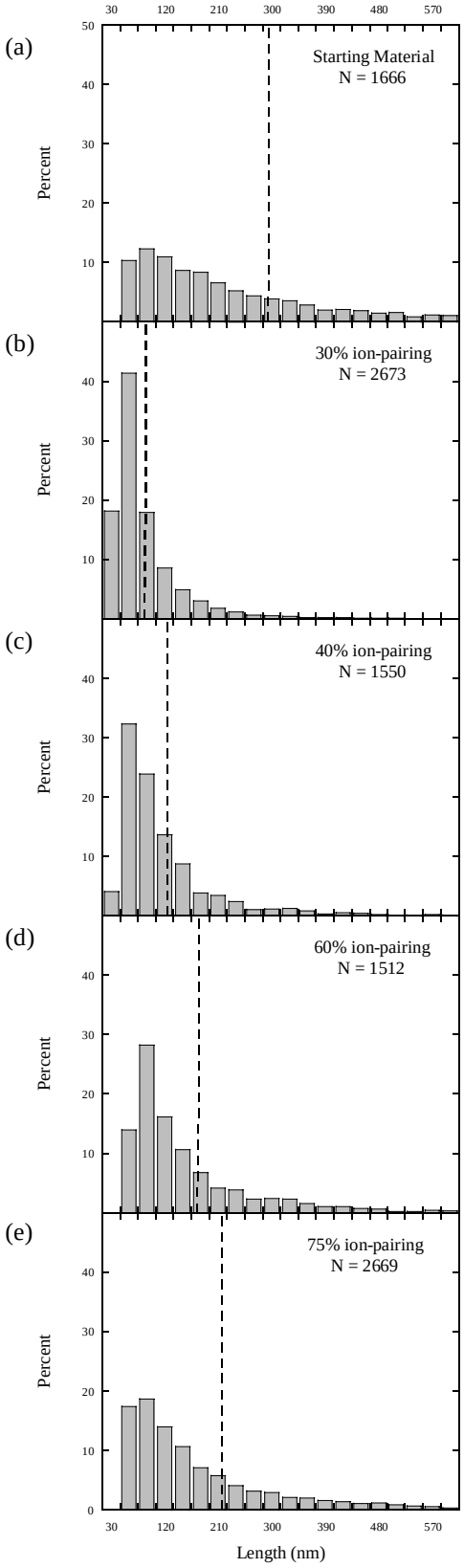

Figure 14. Length distributions of the functionalized SWNTs (a) before extraction and after partial extraction with TOAB corresponding to ion-pairing of (b) 30%, (c) 40%, (d) 60%, and (e) 75%. The dashed lines indicate the average length of the sample.

The length-dependent phase transfer can be understood by considering the attractive interactions between colloidal particles in solution. Colloidal dispersions in organic solvents are typically characterized by the attractive van der Waals interactions between particles and the steric repulsion interaction caused by the brush layer attached to the colloids [20, 21]. Pair-wise summation of the van der Waals attractions results in significantly stronger interactions for larger colloidal particles. This summation results in strong van der Waals interactions for nanotubes, which have been shown to have attractive energies on the order of 36 k_BT/nm [21]. At a given TOAB concentration, the shortest length nanotubes will always have less attractive van der Waals interactions. However, the presence of the organophilic chains creates a steric barrier sufficient to overcome the attractive van der Waals interactions for the smallest length nanotubes [21]. Those nanotubes that cannot be stabilized in the organic layer succumb to the attractive van der Waals interactions, aggregate, and settle to the interface. The addition of more TOA^+ stabilizes and extracts longer nanotubes.

Conclusions

An extraction process has been developed which takes advantage of the considerable attractive force existing between nanotubes. By controlling the concentration of the steric barrier, the length-dependent stabilization of nanotubes in the organic phase can be readily manipulated. The simplicity of the extraction process allows this separation to be easily scaled-up with relatively narrow length distributions.

Suggested Future Work

Ozonated tubes (via PFPE) followed by electron irradiation should be continued to be investigated as a means of cutting nanotubes. The important question to answer will be what fraction of the sample is short, cut tubes versus aggregates. It appears that the amount of irradiation required to induce sidewall damage is minimal. Therefore, future experiments should focus on shorter irradiation times or a lower flux of electrons. The ability to reverse the cross-linking of or the ability to minimize their formation during irradiation will likely significantly increase the yield of this process. The ability to recycle the PFPE solvent and re-use it for ozonation is another important question that will affect the economical viability of this approach.

Publications from work

"Length dependent extraction of single-walled carbon nanotubes", by K. J. Ziegler, D. J. Schmidt, K. N. Shah, E. L. Flor, R. H. Hauge, and R. E. Smalley, Submitted (2005).

"Statistically accurate length measurements of single-walled carbon nanotubes", by K. J. Ziegler, U. Rauwald, Z. Gu, F. Liang, W. E. Billups, R. H. Hauge, and R. E. Smalley, *Journal of Nanoscence and Nanotechnology,* **2007** (*7*), 2917-2921.

"Cutting of Single-Walled Carbon Nanotubes by Ozonolysis" Z. Chen, K. J. Ziegler, J. Shaver, R. H. Hauge, R. E. Smalley *Journal of Physical Chemistry B*, **2006** (*110*), 11624-11627.

"Cutting single-walled carbon nanotubes", by K. J. Ziegler, Z. Gu, J. Shaver, Z. Chen, E. L. Flor, D. J. Schmidt, C. Chan, R. H. Hauge, and R. E. Smalley, *Nanotechnology*, 16, S539-S544 (2005).

"Controlled oxidative cutting of single-walled carbon nanotubes", by K. J. Ziegler, Z. Gu, H. Peng, E. L. Flor, R. H. Hauge, and R. E. Smalley, *Journal of the American Chemical Society*, 127, 1541-1547 (2005).

"Length-Dependent Extraction of Single-Walled Carbon Nanotubes" K. J. Ziegler, D. J. Schmidt, U. Rauwald, K. N. Shah, E. L. Flor, R. H. Hauge, R. E. Smalley *Nano Letters*, **2005** (*5*), 2355-2359.

References

(1) Liu, J.; Rinzler, A. G.; Dai, H. J.; Hafner, J. H.; Bradley, R. K.; Boul, P. J.; Lu, A.; Iverson, T.; Shelimov, K.; Huffman, C. B.; Rodriguez-Macias, F.; Shon, Y. S.; Lee, T. R.; Colbert, D. T.; Smalley, R. E., *Science* **1998,** *280*, 1253.

(2) Collins, P. G.; Bradley, K.; Ishigami, M.; Zettl, A., *Science* **2000,** *287*, 1801.

(3) Chang, H., *J. Am. Chem. Soc.* **1990,** *112*, 4598.

(4) Henning, G. R., *J. Chem. Phys.* **1964,** *40*, 2877.

(5) Chu, X.; Schmidt, L. D., *Surf. Sci.* **1992,** *268*, 325.

(6) Rao, A. M.; Richter, E.; Bandow, S.; Chase, B.; Eklund, P. C.; Williams, K. A.; Fang, S.; Subbaswamy, K. R.; Menon, M.; Thess, A.; Smalley, R. E.; Dresselhaus, G.; Dresselhaus, M. S., *Science* **1997,** *275*, 187.

(7) Chiang, I. W.; Brinson, B. E.; Huang, A. Y.; Willis, P. A.; Bronikowski, M. J.; Margrave, J. L.; Smalley, R. E.; Hauge, R. H., *J. Phys. Chem. B* **2001,** *105*, 8297.

(8) Haddon, R. C.; Raghavachari, K., *Tetrahedron* **1996,** *52*, 5207.

(9) Srivastava, D.; Brenner, D. W.; Schall, J. D.; Ausman, K. D.; Yu, M. F.; Ruoff, R. S., *J. Phys. Chem. B* **1999,** *103*, 4330.

(10) Ramesh, S.; Ericson, L. M.; Davis, V. A.; Saini, R. K.; Kittrell, C.; Pasquali, M.; Billups, W. E.; Adams, W. W.; Hauge, R. H.; Smalley, R. E., *J. Phys. Chem. B* **2004,** *108*, 8794.

(11) Gu, Z.; Peng, H.; Hauge, R. H.; Smalley, R. E.; Margrave, J. L., *Nano Lett.* **2002,** *2*, 1009.

(12) Mickelson, E. T.; Huffman, C. B.; Rinzler, A. G.; Smalley, R. E.; Hauge, R. H.; Margrave, J. L., *Chemical Physics Letters* **1998,** *296*, 188.

(13) Kelly, K.; co-workers, *In preparation* **2005**.

(14) Davis, V. A.; Ericson, L. M.; Parra-Vasquez, A. N. G.; Fan, H.; Wang, Y.; Prieto, V.; Longoria, J. A.; Ramesh, S.; Saini, R. K.; Kittrell, C.; Billups, W. E.; Adams, W. W.; Hauge, R. H.; Smalley, R. E.; Pasquali, M., *Macromolecules* **2004,** *37*, 154.

(15) Zhou, W.; Islam, M. F.; Wang, H.; Ho, D. L.; Yodh, A. G.; Winey, K. I.; Fischer, J. E., *Chem. Phys. Lett.* **2004,** *384*, 185.

(16) Sano, N.; Naito, M.; Chhowalla, M.; Kikuchi, T.; Matsuda, S.; Iimura, K.; Wang, H. L.; Kanki, T.; Amaratunga, G. A. J., *Chemical Physics Letters* **2003,** *378*, 29.

(17) Islam, M. F.; Rojas, E.; Bergey, D. M.; Johnson, A. T.; Yodh, A. G., *Nano Lett.* **2003,** *3*, 269.

(18) O'Connell, M.; Bachilo, S. M.; Huffman, C.; Moore, V. C.; Strano, M. S.; Haroz, E.; Rialon, K. L.; Boul, P.; Noon, W. H.; Kittrell, C.; Ma, J.; Hauge, R. H.; Weisman, R. B.; Smalley, R., *Science* **2002,** *297*, 593.
(19) Moore, V. C.; Strano, M. S.; Haroz, E. H.; Hauge, R. H.; Smalley, R. E., *Nano Letters* **2003,** *3*, 1379.
(20) Shah, P. S.; Holmes, J. D.; Johnston, K. P.; Korgel, B. A., *J. Phys. Chem. B* **2002,** *106*, 2545.
(21) Shvartzman-Cohen, R.; Nativ-Roth, E.; Baskaran, E.; Levi-Kalisman, Y.; Szleifer, I.; Yerushalmi-Rozen, R., *J. Am. Chem. Soc.* **2004,** *126*, 14850.

Soluble Ultra-Short Single-Walled Carbon Nanotubes

Abstract: Soluble, ultra-short (length < 60 nm), carboxylated, single-walled carbon nanotubes (SWNTs) have been prepared by a scalable process. This process, predicated on oleum's (100% H_2SO_4 with excess SO_3) ability to intercalate between individual SWNTs inside SWNT ropes, is a procedure which simultaneously cuts and functionalizes SWNTs using a mixture of sulfuric and nitric acids. The solubility of these ultra-short SWNTs (US-SWNTs) in organic solvents, super acid and water is about 2 wt %. The availability of soluble US-SWNTs could open opportunities for forming high performance composites, blends, and copolymers without inhibiting their processibility.

Introduction

With a Young's modulus of 1000 Gpa,[1] tensile strength of 30 Gpa,[2] ballistic electrical conductance higher than copper,[3] and thermal conductivity equivalent to diamond,[4] single-walled carbon nanotubes (SWNTs) are ranked among the strongest, most electrically conductive, and thermally robust material known. To fully exploit these SWNTs characteristics in macroscopic functional articles such as fibers, films or composites, one must overcome the critical issue of limited solubility that can affect the processibility of SWNT-infused materials. Due to their high aspect ratio and the strong Van der Waals attraction between them, full-length purified SWNTs

tend to aggregate into a dense, robust network of ropes,[5] usually 10-50 nm in diameter and several μm in length, that have limited solubility in either organic, acidic, or aqueous media. Recently, there has been much interest[6-9] in improving the dispersivity of SWNTs in common solvents such as water, *N*-methyl-2-pyrrolidone (NMP) and *N*,*N*-dimethylformamide (DMF) for incorporating them into high performance composites. The objective was to obtain microscopic non-settling, long-term stable dispersions of SWNTs. The primary techniques to achieving this objective include polymer wrapping,[10-13] preparing water soluble surfactant-wrapped individualized SWNTs by using sodium dodecyl sulfate or Triton X-100, accompanied by sonication and high speed centrifugation,[14-17] reduction with alkali metals,[9] and covalent end and/or sidewall functionalization.[18] In addition to the solubility problem, the presence of rigid full-length SWNTs increase the bulk viscosity of composites and blends even when they can be homogeneously dispersed into a host matrix.[7,19,20] This increase in bulk viscosity tends to reduce the processibility of these composites, leading to a limit on the amount of SWNTs that can be used in the composites and therefore constraining performance enhancements that might otherwise be observed. In this study we have developed a new method where purified HiPco SWNTs, or any SWNTs with pristine side-walls, can be cut and functionalized simultaneously. This process produces carboxylated, ultra-short SWNTs (US-SWNTs) with lengths < 60 nm that are readily soluble in polar organic solvents, acids, and water without the aid of sonication, surfactants, or any other means. This high solubility (up to 2 wt % in NMP), coupled with their short length, should enable these US-SWNTs to be dispersed and incorporated as single tubes into other materials to form composites, blends, or block copolymers without significantly diminishing the host's processibility.

The underlying basis for this new method is predicated on oleum's (100% H_2SO_4 with 20% SO_3) ability to effectively intercalate between individual SWNTs inside SWNT ropes.[21] This SWNT-acid intercalation phenomenon is thought to be the result of SWNTs forming charge transfer complexes with the sulfuric acid molecules, a thermodynamically favorable process. Therefore, the current study uses oleum instead of 98% or 96% sulfuric acid used in the previous method which forms only bundles of longer SWNTs.[5] This two-step process consists of (1) dispersing purified or raw SWNTs, as long as these SWNTs have pristine side-walls, in oleum; (2) the introduction of the cutting agent, nitric acid, into the acid-intercalated SWNT dispersion. This protocol affords an efficient, and more uniform cutting and functionalization of SWNTs than ever seen in the past.[5] Prior work showed that the temperature and time dependent oxidation reaction often generated various functional groups (e.g. –COOH, -OH, -C=O, and a small content of sulfur and nitrogen-containing groups) at the open ends and defect sites of the SWNTs structure. However, the prior method was not efficient in that the cutting/functionalization occurred mostly on the surface of the SWNT ropes since 96% H_2SO_4 cannot effectively intercalate into the SWNTs ropes. This resulted in SWNTs that were not functionalized or short enough for dissolution in solvents.

Experimental Section

The purified[22] HiPco[23] SWNTs used in this study were first disentangled to ensure the complete super acid intercalation. This is a multi-step process consisting of (1) soaking of SWNTs (0.3 wt% concentration) in oleum[24] (20% SO_3) overnight so that the intercalation of acid into the tightly entangled network of SWNTs (Figure 1a) will loosen the ropes; (2) use of an

immersion blender such as a rotor/stator operating at high speed (10000 rpm) for up to 72 h to disentangle the network; (3) precipitation and washing of the disentangled SWNTs to rid them of residual acid; and finally, (4) vacuum drying. These disentangled SWNT can be readily intercalated with fuming sulfuric acid.

Experimentally, 400 mg of disentangled SWNTs (0.1 wt%; raw SWNTs can be used but the process is less efficient and impurities from the raw SWNTs might be carried forward), were dispersed in 200 mL oleum (20% SO_3)[24] in an Erlenmeyer flask and stirred overnight under a blanket of dry nitrogen to ensure complete acid-intercalation. Subsequently, a mixture of 100 mL oleum (20% SO_3)[24] and 100 mL 70% HNO_3 was slowly added into the SWNT/oleum dispersion with stirring in an ice bath to maintain the dispersion's temperature as close to room temperature as possible.[24] Afterwards, the SWNTs dispersion was stirred at 65 °C for 2 h. The dispersion was then carefully poured into 1.2 L of Nanopure water (Barnstead Internationals, Dubuque, IA) while being cooled by an external ice bath to room temperature. The black slurry was vacuum filtered onto a 5 μm Teflon® membrane which retained most of the US-SWNTs. After most of the liquid had been pulled through the filter cake, the vacuum line was removed from the flask and the filter cake was stirred with 50 mL of methanol in the Büchner funnel using a spatula; the particles were then coagulated by adding 200 mL diethyl ether and stirring. Little if any organic wash solvent drained through the filter. The aqueous acidic filtrate was poured from the filter flask, vacuum was reapplied and the methanol/diethyl ether wash liquid was pulled through the filter. The filter cake was washed with additional 200 mL portions of diethyl ether until the pH of the filtrate was neutral. The diethyl ether-wet filter cake was transferred to a Petri dish or beaker and the clumps were broken apart with a spatula to provide fine powdered US-SWNTs as the diethyl ether evaporated. The US-SWNTs were vacuum-dried at room temperature overnight,

typically yielding 440 mg of product. The increase in mass is due to the significant increase in oxidation.

Results and Discussion

The striking result of the disentanglement process is illustrated in Figure 1. Before disentanglement, purified HiPco SWNTs exists as tight networks (Figure 1a) of fine (10-20 nm in diameter), entangled, randomly oriented "primordial" ropes. After the process, disentangled, locally aligned super ropes of 50 nm or more in diameter are produced (Figure 1b).

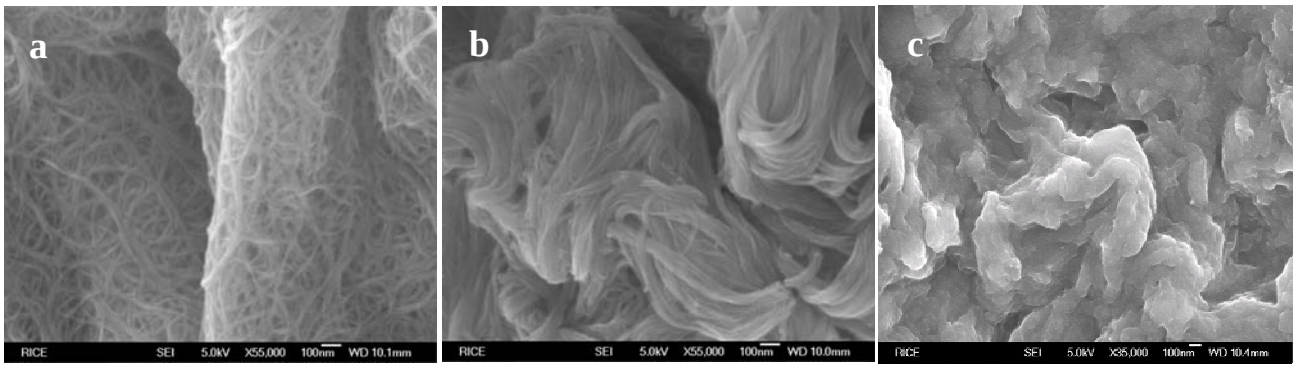

Figure 1. SEM images showing the evolution of purified SWNTs into ultra-short SWNT (US-SWNTs). (a) Tightly entangled network of purified HiPco SWNTs. (b) Aligned super ropes of 50 nm or more in diameter after the disentanglement process. (c) Non-roped structure of US-SWNTs. The scale bar at the bottom of each image is 100 nm.

After the above prescribed oleum / nitric acid treatment, the US-SWNTs (Figure 1c) produced from disentangled SWNTs dissolve spontaneously in polar aprotic solvents such as NMP, DMSO, DMF, alcohol, and in water, without the aid of sonication. However, sonication can help shorten the time of dissolution. Figure 2 shows sequential photographs, taken every 1 min, of this spontaneous dissolution process after dusting US-SWNT powder onto water without stirring.

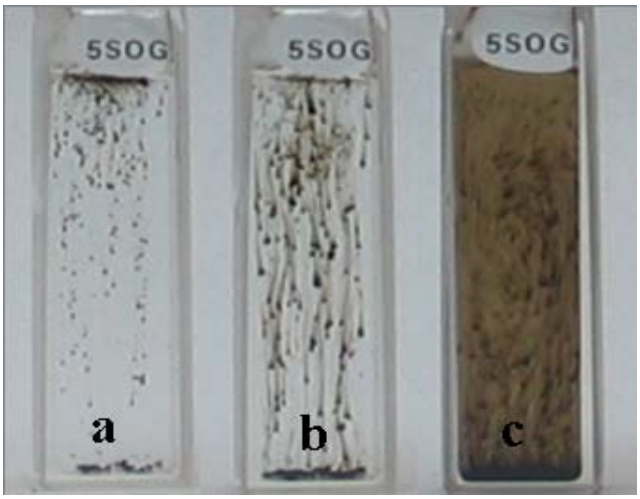

Figure 2. Sequential photographs of the spontaneous dissolution of US-SWNTs in deionized water in quartz curettes. a: 0 min, b: 1 min, c: 2 min

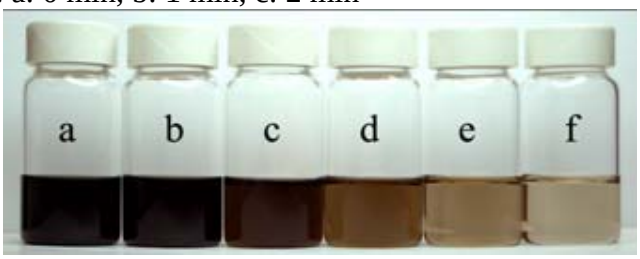

Figure 3. Photograph of US-SWNTs solutions of various concentrations in NMP; a = 500 mg/L, b = 250 mg/L, c = 125 mg/L, d = 62.5 mg/L, e = 31.3 mg/L and f = 15.6 mg/L.

Figure 3 shows photographs of US-SWNTs solutions of various concentrations in NMP. These are true solutions since they are optically transparent and homogeneous. Based on optical microscope examinations, the solubility limit of these US-SWNTs is approximately 2 wt % in NMP, water or super acids. The reason for the high solubility is due to the high level of functionalization on the US-SWNTs. Specifically, these SWNTs are highly carboxylated, and, to a lesser degree, sulfonated. Raman spectra, obtained on a Renishaw Ramascope with 785 cm^{-1} diode laser, of the US-SWNTs are shown in Figure 4a. The results show that these SWNTs are undoubtedly single-walled carbon nanotubes with the characteristic tangential mode (G-band at 1590 cm^{-1}) and the SWNT-unique radial breathing mode (RBM at 100-300 cm^{-1}). For both the disentangled and raw SWNTs, the intensity ratio (D/G ratio) of the disorder mode (D-band at around 1300 cm^{-1}) and the tangential mode is usually less than 1/20, indicating that their

sidewalls are pristine. In comparison, the D/G ratio of the US-SWNTs has increased to close to unity in the case of those produced from disentangled SWNTs. This indicates that there is a high level of sidewall functionalization after the acid treatment. One unexpected result is that the roping peak at 267 cm^{-1} has disappeared for these US-SWNTs (Figure 4b). This surprising result, which infers that these US-SWNTs are no longer roped, is consistent with SEM observation shown in Figure 1c.

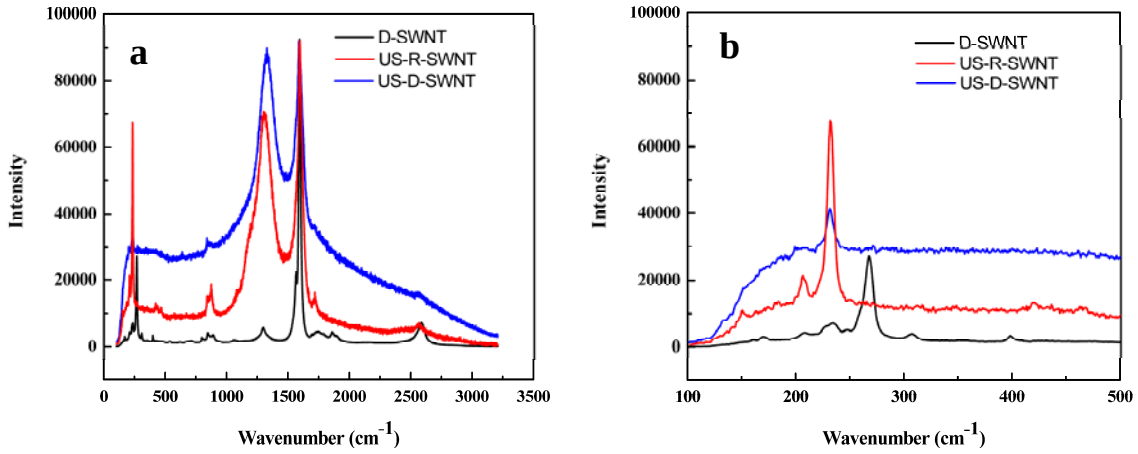

Figure 4. (a) Raman spectra of disentangled SWNT (D-SWNT), ultra-short raw HiPco-derived SWNTs (US-R-SWNT) and ultra-short disentangled SWNT (US-D-SWNT). (b) The detailed radial breath mode indicates the disappearance of the roping mode at 260 cm-1 after cutting.

The X-ray photon-electron spectrum (XPS) (Figure 5a) indicates a high concentration of covalently bonded carboxylic acid groups (-COOH, binding energy ~288 eV) and C=O groups (binding energy ~286 eV) on the surface and ends of these SWNTs. Elemental analysis based on the XPS data shows an approximate stoichiometry of 3:1 C:(COOH) i.e., one of every four SWNT carbons has been functionalized with a 30 % carbon yield from the starting SWNTs. This is in agreement with the thermogravimetric analysis (TGA) results in nitrogen. The functionality is higher than that of a prior study where one of every five SWNT carbons was carboxylated by microwave assisted treatment in acidic mixture.[25] Using our current method, the level of functionalization on the sidewalls, as determined by the D/G ratio, can be varied as function of

duration and/or temperature of the nitric acid treatment, and/or the oleum/nitric acid ratio. By cutting the reaction time of nitric acid from 2 h to 1 h at 65 °C, the D/G ratio decreases to 1/3 indicating the level of functionalization has decreased dramatically. However, by increasing the reaction time to 2.5 h and raising the temperature to 75 °C, the D/G ratio only increases to 1.16, indicating that the level of functionalization may have leveled-off. The sample for FTIR (Nicolet FTIR Infrared Microscopy) spectrum was prepared by dissolving US-SWNTs in a small amount of methanol, mixing with KBr and vacuum drying at 50 °C. The spectrum, shown in Figure 5b, confirms the existence of –COOH and -C=O groups on the sidewalls of the US-SWNTs. The peak at 1707 cm^{-1} is assigned to the C=O stretching mode of the –COOH groups, whereas the broad peak between 2500 and 3300 cm^{-1} is the –OH stretching mode of the –COOH group. The peak at 1583 cm^{-1} is the SWNTs C=C graphitic stretching mode. The peaks observed at 1220 cm^{-1}, 1145 cm^{-1} and 1037 cm^{-1} is due to the C-O stretching. These results, consistent with the Raman data, show the levels of functionalization on these US-SWNTs are high and the functional groups are mostly carboxylic groups.

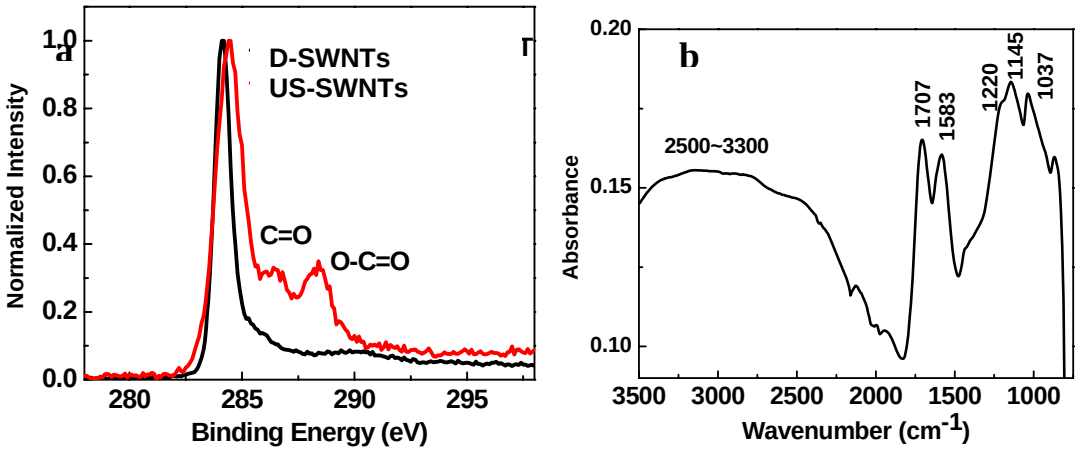

Figure 5. (a) X-ray photoelectron spectroscopy of disentangled SWNTs (D-SWNTs) and US-SWNTs. (b) IR spectra of US-SWNTs (KBr) indicate the existence of carboxylic groups on the sidewalls.

Morphologically, a scanning electron microscopy (SEM) image of the disentangled SWNTs shows the distinct rope structures (Figure 1b), while for US-SWNTs this normal SWNT-characteristic feature (Figure 1c) is absent. One reasonable interpretation is that these US-SWNTs are ultra-short with low aspect ratios and, therefore, do not aggregate into long ropes during the coagulation process. To determine the length of the SWNTs before and after the acid-treatment, atomic force microscopy (AFM) was employed. Purified starting SWNTs used in this study were first alkylated ($C_{12}H_{25}I$) in lithium/liquid ammonia,[18a] and then dispersed in chloroform and spin coated onto mica wafers.[16] In this manner, an unbundled sample of SWNTs is observable. A typical tapping mode AFM image of these purified SWNTs, shown in Figure 6a, indicates that they have average length of 200 nm before the acid-treatment. In contrast, AFM images (Figure 6b) of the US-SWNTs deposited on mica from a water solution indicates that they are indeed ultra short with lengths less than 100 nm, and that they are mostly beyond the resolution of the microscope, which has the tip scale of ~30 nm. To accurately determine the lengths of the US-SWNTs, a high resolution transmission electron microscope (TEM) was employed.

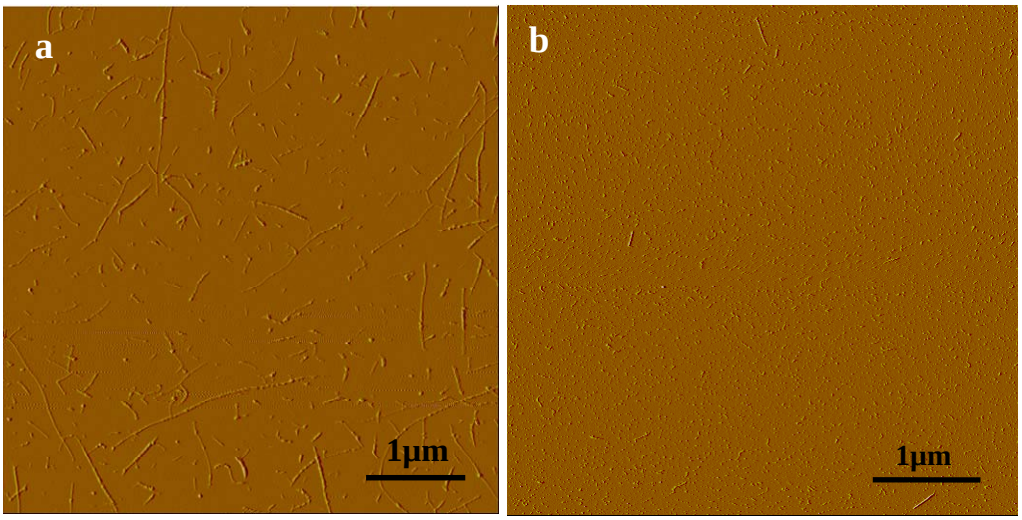

Figure 6. Typical tapping mode AFM images of (a) purified HiPco SWNTs that are alkylated with dodecyl groups to keep them from bundling (b) US-SWNTs.

The TEM sample was prepared by sonicating US-SWNTs in methanol, and the suspension was deposited onto an ultra-thin carbon film on holey carbon grids. Because the contrast between US-SWNTs and carbon film is low, their TEM images have been difficult to obtain. However, some TEM images of US-SWNT with lengths of less than 60 nm are clearly seen in Figure 7. Similar to prior study, the rough edges of the US-SWNTs in the TEM image are indications of the high level of functionalization on the side-walls of the US-SWNT.[6] Also, the inset of Figure 7c shows an isolated, individual US-SWNT on carbon film at 60 nm, which is the longest observed SWNT structure.

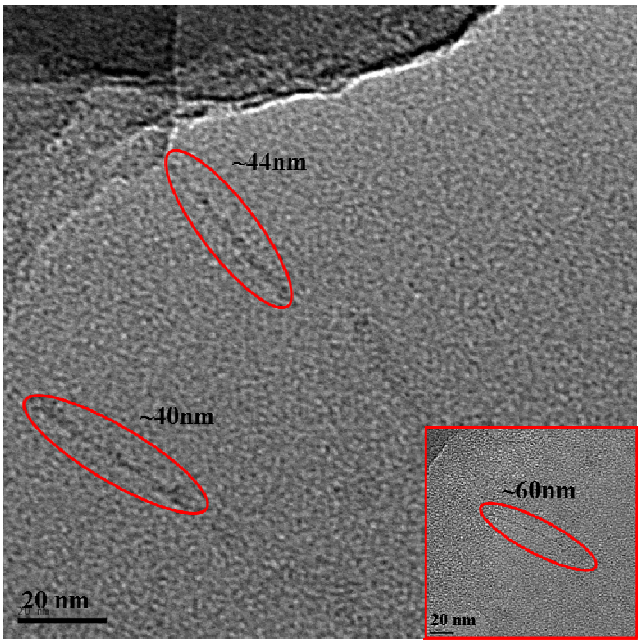

Figure 7. TEM image of US-SWNTs.

Conclusions

In summary, we have developed a new protocol to simultaneously cut and functionalize SWNTs with pristine side-walls to improve their solubility and processibility. This is an efficient and scalable process. This method produces organic solvent, acid, and water soluble, ultra-short

(length < 60 nm), carboxylated SWNTs. The availability of soluble US-SWNTs could open opportunities for forming high performance composites, blends, and copolymers without inhibiting their processibility.

References:

(1) Lu, J. P. *Phys. Rev. Lett.* **1997**, *79*, 1297-1300.

(2) Yu, M-F; Files B. S.; Arepalli, S.; Ruoff, R. S. *Phys. Rev. Lett.* **2000,** *84*, 5552-5555.

(3) Tans, S. J.; Devoret, M. H.; Dai, H.; Thess, A.; Smalley, R. E.; Geerligs, L. J.; Dekker, C. *Nature* **1997**, *386*, 474-477.

(4) Che, J.; Cagin, T.; Goddard,W. A. *Nanotechnology* **2000**, *11*, 65-69.

(5) Liu, J. ; Rinzler, A. G.; Dai, H. J.; Hafner, J. H.; Bradley, R. K.; Boul, P. J.; Lu, A.; Iverson, T.; Shelimov, K.; Huffman, C. B.; Rodriguez-Macias, F.; Shon, Y. S.; Lee, T. R.; Colbert, D. T.; Smalley, R. E. *Science* **1998,** *280*, 1253-1256.

(6) Dyke, C.A.; Tour, J. M. *J. Phys. Chem. A.* **2004**, *108*, 11151-11159.

(7) Tasis, D.; Tagmatarchis, N.; Bianco, A.; Prato, M. *Chem. Rev.* **2006,** *106*, 1105-1136.

(8) Hudson, J. L.; Casavant, M. J.; Tour, J. M. J. *Am. Chem. Soc***. 2004**, *126*, 11158-11159.

(9) Penicaud, A.; Poulin, P.; Derre, A.; Anglaret, E.; Petit, P. *J. Am. Chem. Soc.* **2005**, *127*, 8-9.

(10) Dalton, A. B.; Stephan, C.; Coleman, J. N.; McCarthy, B.; Ajayan, P. M.; Lefrant, S.; Bernier, P.; Blau, W.J.; Byrne, H. J. *J. Phys. Chem. B* **2000**, *104*, 10012-10014.

(11) Star, A.; Stoddart, J. F.; Steuerman, D.; Diehl, M.; Boukai, A.; Wong, E. W.; Yang, X.; Chung, S. W.; Choi, H.; J. R. Heath. *Angew. Chem. Int. Ed.* **2001**, *40*, 1721-1725.

(12) O'Connell, M. J.; Boul, P.; Ericson, L. M.; Huffman, C.; Wang, Y.; Haroz, E.; Kuper, C.; Tour, J. M.; Ausman, K. D.; Smalley, R. E. *Chem. Phys. Lett.* **2001**, *342*, 265-271.

(13) Chen, J.; Liu, J.; Weimer, W.A.; Halls, M. D.; Waldeck, D. H.; Walker, G. C. *J. Am. Chem. Soc.* **2003**, *124*, 9034-9035.

(14) Bonard, J. M.; Stora, T. J.; Salvetat, P.; Maier, F.; Stöckli, T.; Duschl, C.; Forró, L.; Heer, W. A. de.; Châtelain, A. *AdV. Mater.*, **1997**, *9*, 827-831.

(15) Vigolo, B.; Pe´nicaud, A.; Coulon, C. ; Sauder, C.; Pailler, R.; Journet, C.; Bernier, P.; Poulin, P. *Science*, **2000**, *290*, 1331-1334.

(16) Islam, M. F.; Rojas, E.; Bergey, D. M.; Johnson, A. T.; Yodh, A. G. *Nano Lett.*, **2003**, *3*, 269-273.

(17) Moore, V. C.; Strano, M. S.; Haroz, E. H.; Hauge, R. H.; Smalley, R. E. *Nano Lett.*, **2003**, *3*, 1379-1382.

(18) (a) Liang, F.; Sadana, A. K.; Peera, A.; Chattopadhyay, J.; Gu, Z.; Hauge, R. H.; Billups, W. E. *Nano Lett.*, **2004**, *4*, 1257-1260.(b) Georgakilas, V.; Kordatos, K.; Prato, M.; Guldi, D. M.; Holzinger, M.; Hirsch, A. J. *J. Am. Chem. Soc.*, **2002**, *124*, 760-761. (c) Stephenson, J. J.; Hudson, J. L.; Azad, S.; Tour, J. M. *Chem. Mater.* **2006**, *18*, 374-377. (d) Price, B. K.; Hudson, J. L.; Tour, J. M. *J. Am. Chem Soc.* **2005**, *127*, 14867-14870. (e) Dyke, C. A.; Tour, J. M. *Chem. Eur. J.* **2004**, *10*, 812-817.

(19) Gong, X.Y.; Liu, J.; Baskaran, S.; Voise, R. D.; Young, J. S. *Chem. Mater.* **2000**, *12*, 1049-1052.

(20) Cui, S.; Canet, R.; Derre, A.; Couzi, M.; Dehaes, P. *Carbon* **2003**, *41*, 797-809.

(21) Ericson, L. M. *et al.*, *Science* **2004,** *305*, 1447-1450.

(22) Xu, Y. Q.; Peng, H. Q.; Hauge, R. H.; Smalley, R. E. *Nano Letters* **2005**, *5*, 163-168.

(23) Bronikowski, M. J.; Willis, P. A.; Colbert, D. T.; Smith, K. A.; Smalley, R. E. *J. Vac. Sci. & Tech. A-Vac. Surf. & Films* **2001**, *19*, 1800-1805.

(24) **CAUTION!** Oleum and 70% nitric acid are extremely hazardous materials that should be handled with utmost care. Users should wear an acid-proof apron, heavy gloves, safety glasses, a face shield, and all operations should be done in a fume hood when handling these reagents.

(25) Wang, Y.; Iqbal, Z.; Mitra, S. J *J. Am. Chem. Soc.*, **2006**, *128*(1), 95-99.